Hindawi
Journal of Nanomaterials
Volume 2018, Article ID 1234506, 9 pages
https://doi.org/10.1155/2018/1234506

Research Article

A Comparison of Pd^0 Nanoparticles and Pd^{2+} Modified $Bi_2O_2CO_3$ for Visible Light-Driven Photocatalysis

Xiangchao Meng,[1] Zizhen Li,[1] Nan Yun,[1] and Zisheng Zhang [1,2]

[1] *Department of Chemical and Biological Engineering, University of Ottawa, 161 Louis Pasteur Private, Ottawa, ON, Canada K1N 6N5*
[2] *College of Chemical Engineering, Qingdao University of Science & Technology, Qingdao 266042, China*

Correspondence should be addressed to Zisheng Zhang; zzhang@uottawa.ca

Received 22 September 2017; Accepted 21 November 2017; Published 1 January 2018

Academic Editor: Sergio Obregón

As two effective approaches to increase the visible light-absorption capacities of photocatalysts, ion doping and metallic nanoparticles loading are compared in this work. Palladium was selected to modify $Bi_2O_2CO_3$. Compared to dispersing palladium nanoparticles on the photocatalyst surface, it was more effective for the method of doping with palladium to shift the energy level within the bandgap of $Bi_2O_2CO_3$ in improving its photocatalytic activity under visible light. This might be because doping with Pd^{2+} narrows the band gap of $Bi_2O_2CO_3$ so as to increase the absorption capacity of visible light photons. Pd nanoparticles on the other hand can absorb photons to produce electrons which are then utilized by $Bi_2O_2CO_3$ for photocatalytic reactions. Different mechanisms resulted in significant differences, and this work provides solid evidence that ion doping may be a more effective method to improve the photocatalytic activity of $Bi_2O_2CO_3$.

1. Introduction

Photocatalysis is an advanced oxidation process, which has been extensively studied in various areas. Two of its primary applications are hydrogen evolution via water splitting and decomposition of organic pollutants [1, 2]. Bismuth-based semiconductors (BBS) have been widely studied and applied to photocatalysis [3]. Compared to TiO_2, which is a pioneer in the field of photocatalysis, and not to mention the most widely studied, BBS (e.g., Bi_2WO_6, BiOBr, Bi_2MoO_6, $BiVO_4$) exhibits a greater visible light-response [4–7]. However, among various BBS, there are some semiconductors with wide band gaps that may only be activated by UV light, such as $Bi_2O_2CO_3$, $BiOIO_3$, BiOCl, and $BiPO_4$ [8–11]. To improve their visible light-driven photocatalytic activities, approaches are adopted, mainly including doping and preparation of plasmonic photocatalyst [12, 13].

$Bi_2O_2CO_3$, which is a lamellar compound, has a crystal structure consisting of $(Bi_2O_2)^{2+}$ layers interleaved by slabs comprising CO_3^{2-} groups [8]. The band gap of $Bi_2O_2CO_3$ is approximately 3.46 eV, which is wider than that of TiO_2 (~3.2 eV). This indicates that only irradiation with a wavelength lower than 358 nm may be absorbed by pure $Bi_2O_2CO_3$. Modifications are therefore required to make $Bi_2O_2CO_3$ visible light-response. Doping with elemental N, S, and Br has been reported with improved visible light-induced photocatalytic activity [14–16]. Heterojunctions such as Ag_2O-$Bi_2O_2CO_3$ have been also implemented [17]. Another popular approach to improve the visible light-driven photoactivity is by surface deposition of noble metal nanoparticles on a photocatalyst. Peng et al. have reported on $Bi_2O_2CO_3$ modified with Ag and Au nanoparticles, showing an enhanced visible light-driven photocatalytic activity [18, 19]. Our group recently found that palladium nanoparticles were also promising candidates to improve the photocatalytic activities of semiconductors [20–23]. However, most of our reported work focused on using palladium to improve the photocatalytic activity of a semiconductor which is visible light-responsive without modification. As for the intrinsic properties of $Bi_2O_2CO_3$, its band gap is too wide to be visible light-responsive. Palladium nanoparticles may be introduced to the surface of $Bi_2O_2CO_3$, and due to the resultant surface

plasmon resonance (SPR) effect, more visible light photons may be absorbed by $Bi_2O_2CO_3$ [24, 25]. Palladium may also be doped into the lattice of $Bi_2O_2CO_3$ with dopant levels within its band gap. The comparison between loading with Pd nanoparticles and doping with Pd to improve the visible light-driven photocatalytic activity of $Bi_2O_2CO_3$ may be interesting to guide the adoption of a modification method.

In this work, both palladium nanoparticles and palladium ions are deposited/doped onto/into $Bi_2O_2CO_3$, respectively. Activity was evaluated with regard to the degradation of Rhodamine B under visible light irradiation. Mechanisms were also proposed and discussed.

2. Experimental

2.1. Preparation. Pure $Bi_2O_2CO_3$ was prepared using a hydrothermal method. Typically, 8 mmol of $Bi(NO_3)_3 \bullet 5H_2O$ was first dissolved in 20 mL of HNO_3 solution (1 mol/L) to form a clear solution. Then, 60 mL of Na_2CO_3 solution (0.8 mol/L) was added dropwise to the aforementioned solution. After magnetically stirring for 30 min, the mixture was transferred to a 100-mL Teflon-lined autoclave (Parr Instrument Company) and heated at 180°C for 24 h. After the autoclave was allowed to naturally cool down to room temperature, the $Bi_2O_2CO_3$ precipitates were separated by filtration and washed once with ethanol then twice with distilled deionized water (DDW). The washed powder samples were then dried at 60°C for 12 h and collected.

Pd nanoparticles were photoreduced on the surface of $Bi_2O_2CO_3$. In a typical process, $Bi_2O_2CO_3$ and $PdCl_2$ were first dispersed in a solution containing 40 mL of DDW and 5 mL of ethanol under ultrasonication for 30 min. The mixture was then illuminated under ultraviolet-light (UV) (40 W Reflector Blacklight at 353 nm wavelength from Philips) for 1 h with magnetically stirring. The resultant powder samples were then dried, collected, and labelled as Pd(0)-Bi. For preparation of Pd^{2+} doped $Bi_2O_2CO_3$ composites, $Bi_2O_2CO_3$ and $PdCl_2$ were first dispersed in 40 mL of DDW and magnetically stirred for 24 h. Next, the mixture was dried at 100°C for 12 h. The dried powder samples were then annealed at 450°C for 1 h in air. The resultant powder samples were collected and labelled as Pd(II)-Bi. The quantities of Pd^0 and Pd^{2+} in Pd(0)-Bi and Pd(II)-Bi were both at 1.0 wt%.

2.2. Characterization. X-ray diffraction (XRD) analysis was performed on a Rigaku Ultima IV Diffractometer with Cu Kα radiation (λ = 0.15418 nm) at 40 kV and 44 mA. Elemental composition and chemical states on the sample surface were measured using XSAM-800 X-ray Photoelectron Spectroscopy (XPS). Transmission electron microscopy (JEM-2100F, JEOL) was applied to study the morphologies of the prepared samples. The fitting results of XPS curves were analyzed with CASAXPS (version: 2.3.16PR1.6) and XPSPEAK (version: 4.1). Shirley backgrounds were applied for all curve fittings of the XPS peaks. The specific surface area, pore volume, and average pore size were obtained from N_2 sorption isotherms at 77 K, using automatic adsorption apparatus and measurement systems (ASAP 2020, Micromeritics and Nova 4200E, Quantachrome). The Brunauer, Emmett, and Teller (BET) surface area of the samples were calculated using multipoint estimation. Optical properties of the samples were investigated using a Thermo Evolution 300 spectrophotometer. The Fourier Transform Infrared Spectroscopy (FTIR) was performed using a Cary 630 (Agilent Technologies). Electrochemical properties of prepared samples were performed on a CHI 604E electrochemical analyzer (CH Instruments Inc., USA) with a platinum wire as a counter electrode, a calomel reference electrode, and a working electrode. The working electrode was composed of indium tin oxide (ITO, 75 × 25 × 1.1 mm, 15–25 Ω, Sigma-Aldrich Canada Co.) glass coated with the prepared samples. The electrochemical impedance spectroscopies (EIS) were recorded with frequencies in the range of 1–1000000 Hz and a sinusoidal wave of 5 mV. The electrolyte was Na_2SO_4 with a concentration of 0.05 mol/L. The quantum-mechanical calculations were performed on the basis of the density functional theory (DFT) [26]. The generalized gradient approximation (GGA) was applied to exchange-correlation effects [27]. The open access software Quantum ESPRESSO was used, which utilizes pseudopotentials to describe electron-ion interactions and represents electronic wave functions using a plane-wave basis set [28]. The kinetic energy cut-off was set to 300 eV.

2.3. Photocatalytic Activity Tests. The photocatalytic activities of prepared samples under visible light irradiation were investigated with regard to the degradation of Rhodamine B (RhB). A 500 mL beaker served as the reactor with a cooling jacket to maintain the temperature at approximately 20°C. The light source was a 300-W halogen tungsten projector lamp (Ushio) with a UV cut-off (Kenko Zeta, transmittance > 90%) to filter out irradiation with wavelengths below 410 nm. The irradiation intensity on the surface of the solution was measured by a quantum meter (Biospherical QSL-2100, 400 < λ < 700 nm) and was found to be 1.1×10^{-2} Einstein m^{-2} s^{-1}. In each test, 100 mL of RhB solution (10 mg/L) was mixed with 0.05 g of prepared photocatalyst composites. Photocatalytic tests were each performed for 60 min, and aliquots were drawn periodically. The supernatants were analyzed using a UV-Visible absorption spectrometer (Genesys 10 UV) for RhB. The total organic carbon (TOC) was evaluated on an Apollo 9000 TOC analyzer equipped with a nondispersive infrared (NDIR) detector. The combustion temperature was fixed at 750°C.

3. Results and Discussions

3.1. Crystal Structures and Compositions Analysis. Crystal structures were studied using XRD (Figure 1). All observed peaks may be identified, and it can be seen that an orthorhombic $Bi_2O_2CO_3$ crystal structure (Pna21(33), cell = $5.468 \times 27.320 \times 5.468$ Å^3) [29] was successfully prepared. No apparent differences were observed after modification with either Pd^0 or Pd^{2+}, indicating that the crystal structure of $Bi_2O_2CO_3$ was negligibly influenced by the modification process. The chemical bonding of composites was observed by FTIR measurements (Figure 2). The peaks absorption at

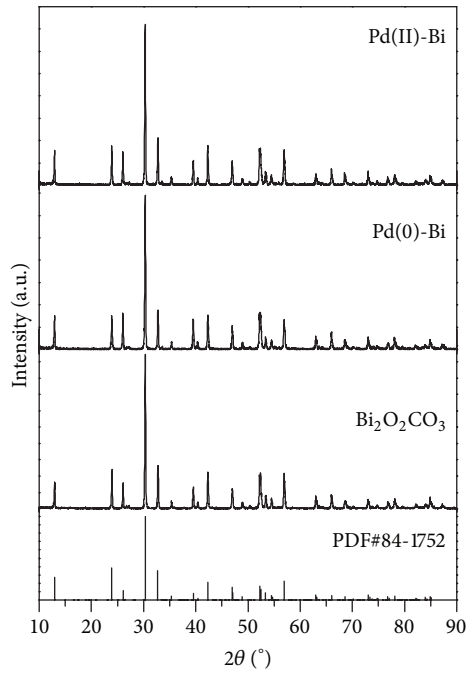

FIGURE 1: XRD patterns for pure $Bi_2O_2CO_3$, Pd(0)-Bi, and Pd(II)-Bi composites.

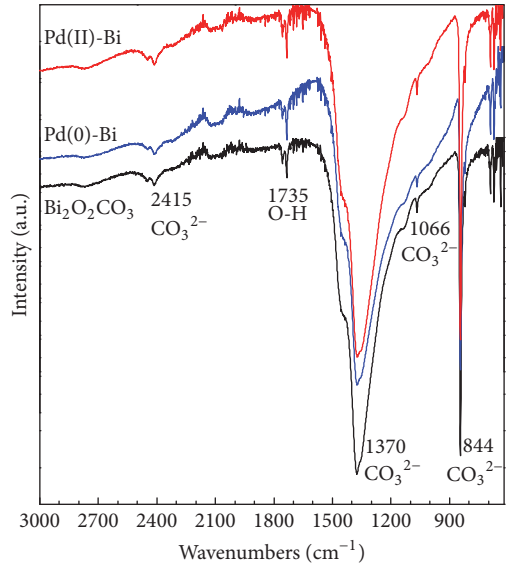

FIGURE 2: FTIR for pure $Bi_2O_2CO_3$, Pd(0)-Bi, and Pd(II)-Bi composites.

2415, 1370, 1066, and 844 cm^{-1} may be derived from the vibrations of CO_3^{2-} group [8, 30]. The peak at 1735 cm^{-1} may be attributed to the stretching and deformation vibrations of the O-H groups in physisorbed/chemisorbed water molecules [20]. No other impurities were detected, confirming a high purity of $Bi_2O_2CO_3$. As for the low content of palladium in Pd(0) and Pd(II) modified $Bi_2O_2CO_3$, no characterization peak for palladium was observed.

To confirm the presence of palladium in the Pd-$Bi_2O_2CO_3$ composites, XPS was employed. The XPS high-resolution orbital scan of Pd 3d, shown in Figure 3(a), highlights the differences between Pd(0)-Bi and Pd(II)-Bi. In particular, two peaks at binding energies (BE) of 342.5 and 337.2 eV were each observed in both spectra, possibly derived from the palladium precursor, $PdCl_2$. The peaks located at 340.3 and 335.4 eV in the spectrum of Pd(0)-Bi may be assigned to metallic palladium nanoparticles (Pd^0), whereas peaks at 343.5 and 338.8 eV in the spectrum of Pd(II)-Bi may be assigned to an O-Pd-O structure [31]. This suggests that Pd^{2+} may be doped into the lattice of $Bi_2O_2CO_3$. In the XPS spectra of Cl 2p (Figure 3(b)), one set of doublet peaks in the spectrum of Pd(0)-Bi further confirms the presence of $PdCl_2$ on the surface. In addition to the peaks ascribed to $PdCl_2$, another set of doublet peaks were also observed, which was probably due to the presence of Cl doped in the lattice of $Bi_2O_2CO_3$. It should be noted that a BiOCl-$Bi_2O_2CO_3$ heterostructure may be formed in the Pd(II)-Bi composites [32].

3.2. Morphologies, Optical Properties, and Photocatalytic Activity Tests. The morphology of Pd(0)-Bi was investigated using TEM imaging and shown in Figure 4. Palladium nanoparticles were successfully dispersed on the surface of the photocatalyst and may be activated by visible light irradiation due to the local surface plasmon resonance effect (SPR), which was confirmed in the optical properties study (Figure 6). Nitrogen sorption isotherms were illustrated in Figure 5 for prepared samples. The specific surface areas for $Bi_2O_2CO_3$, Pd(II)-Bi, and Pd(0)-Bi composites are calculated using multipoint estimation as 29.7, 29.3, and 27.2 m^2/g, respectively. It indicates the doping with Pd^{2+} negligibly influenced the specific surface area of $Bi_2O_2CO_3$. However, the loading of palladium nanoparticles on the surface may block the slit-shaped pores, which may lead to the reduction in photocatalytic activity of $Bi_2O_2CO_3$. In the diffused reflectance spectra (DRS) as shown in Figure 6(a), a steep increase was observed for pure $Bi_2O_2CO_3$, when the wavelength falls below 358 nm. This indicates that a band gap transition occurs at a wavelength of 358 nm. The corresponding band gap value calculated with the Kubelka-Munk function was about 3.46 eV. After modification with palladium nanoparticles, no red-shift was observed, and the band gap transition occurred at the same wavelength. A great increase in the visible light region was clearly observed after depositing palladium nanoparticles onto the surface, which may be a result of the SPR effect of palladium nanoparticles on the surface. As shown in Figure 6(b), it confirms that the palladium nanoparticles are capable of harvesting photons in visible light region. For the spectrum of Pd(II)-Bi, a negligible red-shift occurred for the band transition, and the absorption capacity in the visible light region was improved, possibly due to the Pd^{2+} dopant which would add doping levels within the band gap of $Bi_2O_2CO_3$ [12]. Both Pd^0 and Pd^{2+} modifications result in $Bi_2O_2CO_3$ becoming visible light-responsive.

The photocatalytic activity was evaluated with regard to the degradation of RhB, the results of which are depicted

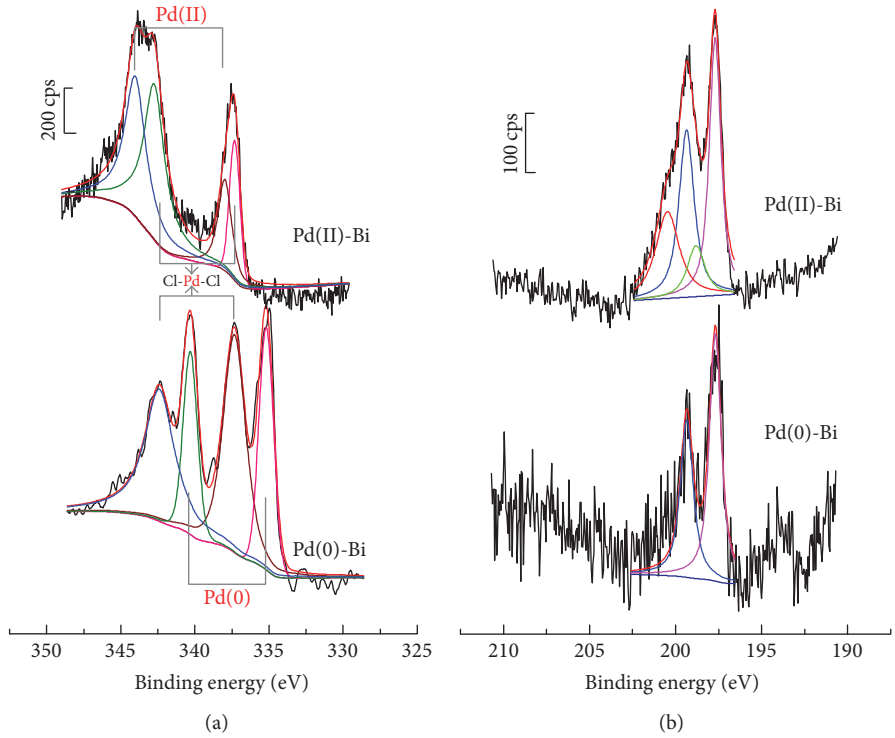

Figure 3: High-resolution orbital scans of (a) Pd 3d and (b) Cl 2p for Pd(0)-Bi and Pd(II)-Bi composites.

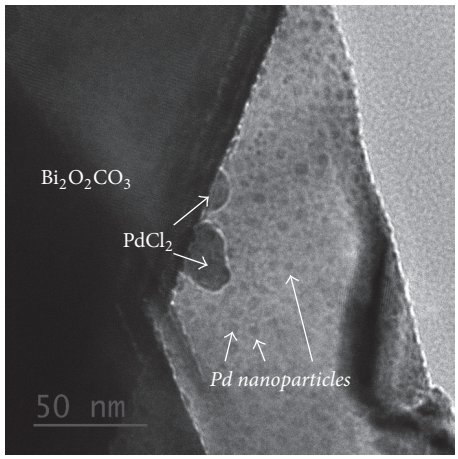

Figure 4: TEM image of Pd(0)-Bi composite.

in Figure 7. About 6.2% of initial RhB was removed by photolysis over 60 min. For the adsorption, about 8.8, 13.0, and 10.1% of RhB were adsorbed on pure $Bi_2O_2CO_3$, Pd(0)-Bi, and Pd(II)-Bi composites over 30 min in the absence of light, respectively. With turning on the lamp to initialize the photocatalytic process, it can be found that about 38.5% of initial RhB was removed over 60 min in the presence of pure $Bi_2O_2CO_3$ under visible light irradiation, as $Bi_2O_2CO_3$ is visible light-irresponsive. The removal of RhB may be attributed to the photosensitization of RhB [33–35]. After deposition of palladium nanoparticles on the surface of $Bi_2O_2CO_3$, a slight increase in the photocatalytic removal of RhB was observed. The increase may be due to an improvement in the absorption of visible light photons by Pd nanoparticles on the surface [36, 37]. However, the intrinsic band gap of $Bi_2O_2CO_3$ is too wide to be visible light-responsive, and so the enhancement by palladium nanoparticles was limited. For Pd(II)-Bi composites, a significant increase in the photocatalytic removal of RhB was observed. Specifically, all of RhB was completely removed over 60 min in the presence of Pd(II)-Bi composites under visible light irradiation. This great improvement may be attributed to the greatly increased visible light photons absorbing for Pd^{2+} modified $Bi_2O_2CO_3$. The dopant level within band gap of $Bi_2O_2CO_3$ not only confers it visible light-responsive, but also facilitates the separation of photogenerated charge carriers [38]. As for the TOC (Figure 8), about 3.8, 9.2, and 25.2% of initial TOC were removed over 60 min for systems with pure $Bi_2O_2CO_3$, Pd(0)-Bi, and Pd(II)-Bi composites, respectively. This further confirms that Pd doping may be more effective in improving the photocatalytic oxidation of organics in water by $Bi_2O_2CO_3$, with longer reaction time required to completely remove TOC [39].

3.3. Mechanism Exploration. The electrochemical impedance spectra (EIS) Nyquist plots were illustrated in Figure 9. Only one arc was observed for all plots, indicating the photocatalytic process may be a simple electrode reaction. The diameter of the arc was in positive proportion to the resistance value of the electron transfer on the electrode. An equivalence circuit was also depicted in the inset of Figure 9, where R_s and R_{ct} represent resistance for the solution and resistance to the electron transfer on the electrode,

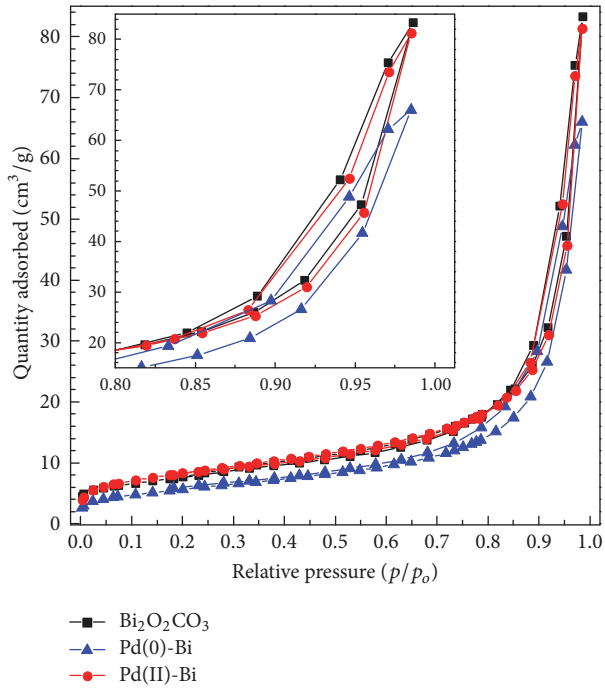

FIGURE 5: N_2 adsorption-desorption isotherm of pure $Bi_2O_2CO_3$, Pd(0)-Bi, and Pd(II)-Bi composites (the inset shows the enlarged isotherm at p/p_0 = 0.80–1.00).

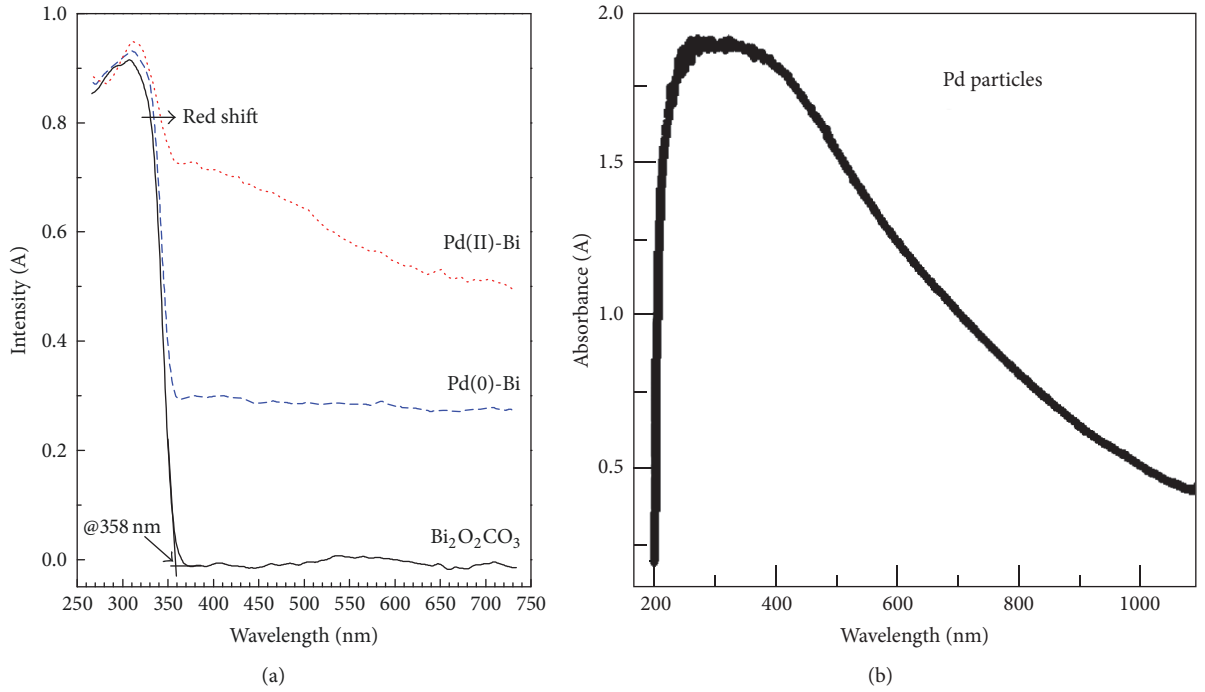

FIGURE 6: (a) DRS for pure $Bi_2O_2CO_3$, Pd(0)-Bi, and Pd(II)-Bi composites and (b) UV-Visible spectrum for palladium nanoparticles.

respectively. R_s for all electrodes are similar, as all electrodes immersed in the same solution. R_{ct} for $Bi_2O_2CO_3$, Pd(0)-Bi, and Pd(II)-Bi electrodes are estimated to be 65.32, 57.49, and 16.33 kΩ, respectively. These results suggest the recombination of photogenerated charge carriers was suppressed with Pd(0) and Pd(II) modification, and Pd(II) doping was more effective compared to Pd(0) loading.

To study the mechanism for doping of Pd into $Bi_2O_2CO_3$, a palladium atom was added to the lattice of $Bi_2O_2CO_3$ as shown in Figure 10(a). Simulated results for pure $Bi_2O_2CO_3$

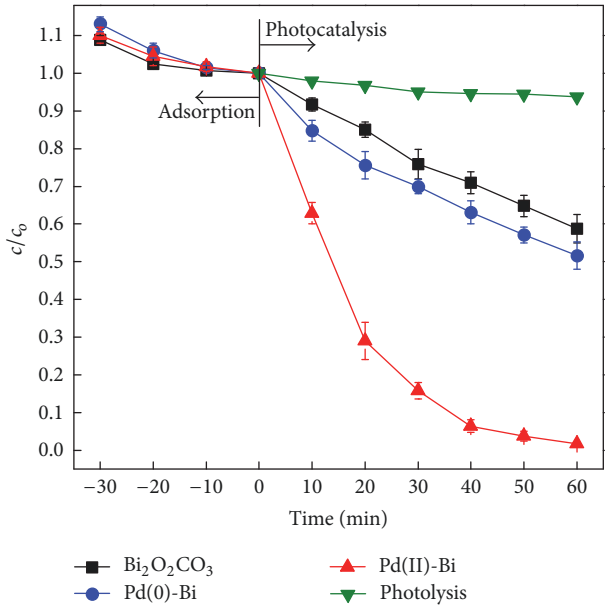

FIGURE 7: Photocatalytic degradation of RhB in the presence of various prepared samples.

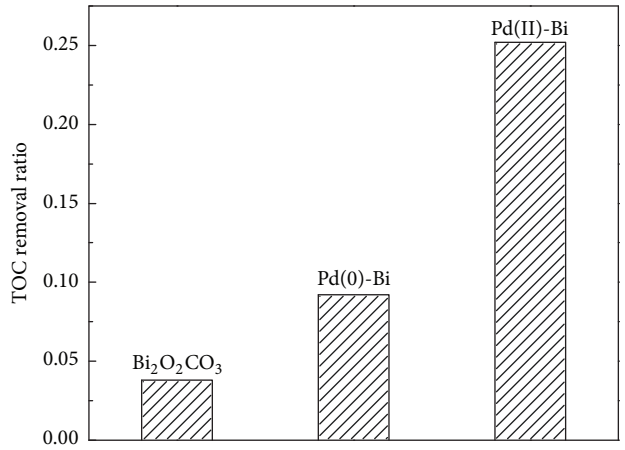

FIGURE 8: TOC removal ratio for photocatalytic degradation of RhB in presence of various photocatalysts.

and Pd(II)-Bi composites were plotted in Figure 10(b). The calculated band gap for pure $Bi_2O_2CO_3$ was about 2.45 eV, which is lower than experimental result of 3.46 eV. This is a general phenomenon between the simulated and experimental results in the estimation of band gaps. With doping Pd^{2+} in the lattice of $Bi_2O_2CO_3$, several dopant energy levels were added within the band gap of $Bi_2O_2CO_3$. And these dopant levels are sufficiently overlapped with the band states of $Bi_2O_2CO_3$, favoring the transfer of charge carriers [38]. This agrees well with DRS results, and the absorption of visible light photons was greatly improved due to these dopant levels.

Proposed mechanisms for an enhanced photocatalytic activity via deposition of palladium nanoparticles and doping of Pd^{2+} into $Bi_2O_2CO_3$ were illustrated in Figures 11(a) and 11(b), respectively. Typically, for Pd(0)-Bi composites,

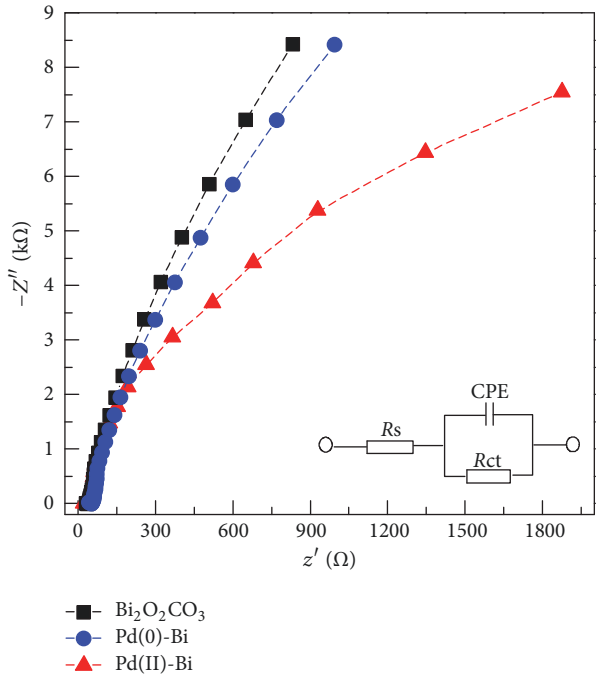

FIGURE 9: EIS Nyquist plots of prepared samples (inset: equivalent circuit).

palladium nanoparticles on the surface may be capable of capturing visible light photons, due to the SPR effect. However, the support, $Bi_2O_2CO_3$, was not in itself visible light-response. Comparatively, when palladium is doped into the lattice with dopant levels within band gaps of $Bi_2O_2CO_3$, visible light may be absorbed by the support to generate electrical charge carriers [38]. This is consistent with our experiments suggesting that doping is a more effective strategy to improve the activity of a photocatalyst that has a low visible light-responsivity.

4. Conclusions

Two main approaches to improve the visible light-driven photocatalytic activity, namely nanoparticle deposition and ion doping, have been extensively adopted in practice. A comparison of these two approaches in this work via combining palladium with $Bi_2O_2CO_3$ has been conducted. It can be concluded that both palladium nanoparticle deposition as well as palladium doping are capable of improving the absorption of visible light photons, although the extents of these improvements are drastically different. The band gap of $Bi_2O_2CO_3$ was negligibly influenced by the deposition of Pd nanoparticles, as visible light photons cannot be absorbed by $Bi_2O_2CO_3$, being absorbed solely by palladium nanoparticles at the photocatalyst surface. The activated electrons may inject into the conduction band of $Bi_2O_2CO_3$ due to the difference in work functions between palladium and $Bi_2O_2CO_3$; however, this improvement is limited. In contrast, palladium doping at several dopant levels within the band gap of $Bi_2O_2CO_3$ was capable of conferring visible light-responsivity to the support. This improvement appears to be significant.

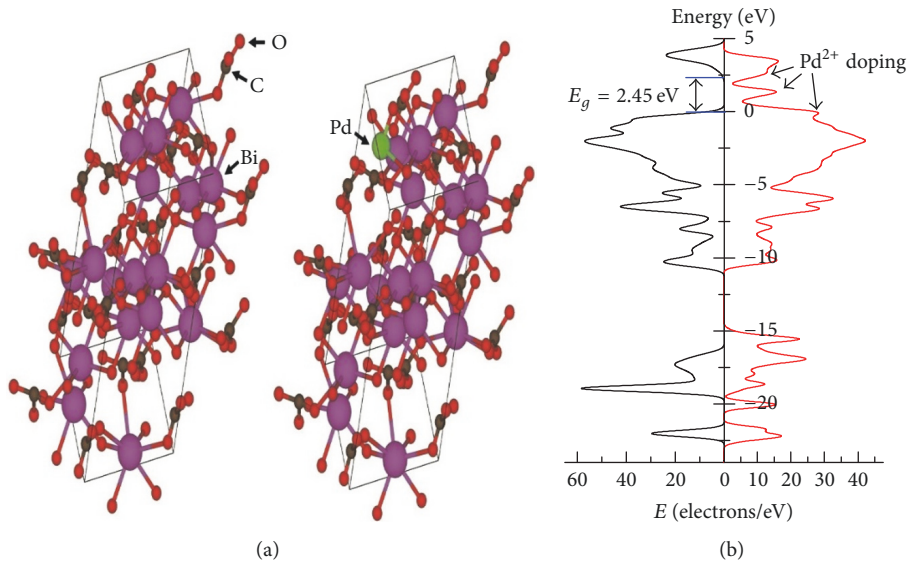

Figure 10: (a) Crystal structures and (b) total density of states of $Bi_2O_2CO_3$ with and without Pd(II) doping [28, 40].

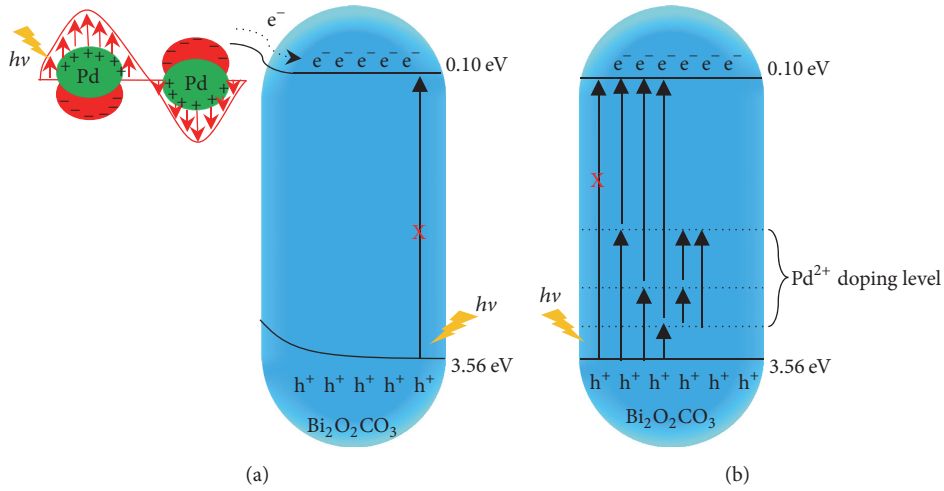

Figure 11: Proposed mechanism for the photocatalytic degradation process in the presence of (a) Pd(0)-Bi and (b) Pd(II)-Bi.

This work infers that noble metal nanoparticles may be more effective in improving the photocatalytic activity of a semiconductor that is already visible light-responsive prior to modification. Improvements from the deposition of metallic nanoparticles on the surface are limited by the intrinsic properties of the support. This work sheds a light on the importance of considering ion doping in the modification of a photocatalyst.

Conflicts of Interest

The authors declare no actual or potential conflicts of interest.

Acknowledgments

This work was financially supported by the Natural Sciences and Engineering Research Council of Canada. Xiangchao Meng was the recipient of a scholarship from the China Scholarship Council (CSC) for the duration of this work. The authors would like to acknowledge Dr. Alexander Mommers and Yun Liu at the Center for Catalysis Research and Innovation (CCRI), University of Ottawa, for their help with materials characterization.

References

[1] D. S. Bhatkhande, V. G. Pangarkar, and A. A. Beenackers, "Photocatalytic degradation for environmental applications—a review," *Journal of Chemical Technology and Biotechnology*, vol. 77, no. 1, pp. 102–116, 2002.

[2] M. Ni, M. K. H. Leung, D. Y. C. Leung, and K. Sumathy, "A review and recent developments in photocatalytic water-splitting using TiO2 for hydrogen production," *Renewable & Sustainable Energy Reviews*, vol. 11, no. 3, pp. 401–425, 2007.

[3] X. Meng and Z. Zhang, "Bismuth-based photocatalytic semiconductors: introduction, challenges and possible approaches," *Journal of Molecular Catalysis A: Chemical*, 2016.

[4] M. Shang, W. Wang, L. Zhang, and H. Xu, "Bi_2WO_6 with significantly enhanced photocatalytic activities by nitrogen doping," *Materials Chemistry and Physics*, vol. 120, no. 1, pp. 155–159, 2010.

[5] H. Li, G. Liu, and X. Duan, "Monoclinic $BiVO_4$ with regular morphologies: hydrothermal synthesis, characterization and photocatalytic properties," *Materials Chemistry and Physics*, vol. 115, no. 1, pp. 9–13, 2009.

[6] L. Xie, J. Ma, and G. Xu, "Preparation of a novel Bi2MoO6 flake-like nanophotocatalyst by molten salt method and evaluation for photocatalytic decomposition of rhodamine B," *Materials Chemistry and Physics*, vol. 110, no. 2-3, pp. 197–200, 2008.

[7] H. Li, C. Liu, K. Li, and H. Wang, "Preparation, characterization and photocatalytic properties of nanoplate Bi_2MoO_6 catalysts," *Journal of Materials Science*, vol. 43, no. 22, pp. 7026–7034, 2008.

[8] H. Cheng, B. Huang, K. Yang et al., "Facile template-free synthesis of Bi2O2CO3 hierarchical microflowers and their associated photocatalytic activity," *ChemPhysChem*, vol. 11, no. 10, pp. 2167–2173, 2010.

[9] K. L. Zhang, C. M. Liu, F. Q. Huang, C. Zheng, and W. D. Wang, "Study of the electronic structure and photocatalytic activity of the BiOCl photocatalyst," *Applied Catalysis B: Environmental*, vol. 68, no. 3-4, pp. 125–129, 2006.

[10] X. M. Qi, M. L. Gu, X. Y. Zhu et al., "Fabrication of BiOIO3 nanosheets with remarkable photocatalytic oxidation removal for gaseous elemental mercury," *Chemical Engineering Journal*, vol. 285, pp. 11–19, 2016.

[11] C. Pan and Y. Zhu, "New Type of $BiPO_4$ oxy-acid salt photocatalyst with high photocatalytic activity on degradation of dye," *Environmental Science & Technology*, vol. 44, pp. 5570–5574, 2010.

[12] Y. Zhou, Z. Zhao, F. Wang et al., "Facile synthesis of surface N-doped Bi2O2CO3: Origin of visible light photocatalytic activity and in situ DRIFTS studies," *Journal of Hazardous Materials*, vol. 307, pp. 163–172, 2016.

[13] L. Jin, G. Zhu, M. Hojamberdiev et al., "A Plasmonic Ag–AgBr/$Bi_2O_2CO_3$ Composite Photocatalyst with Enhanced Visible-Light Photocatalytic Activity," *Industrial & Engineering Chemistry Research*, vol. 53, pp. 13718–13727, 2014.

[14] Y. Liu, S. Yu, Z. Zhao, F. Dong, X. A. Dong, and Y. Zhou, "N-Doped $Bi_2O_2CO_3$/graphene quantum dot composite photocatalyst: enhanced visible-light photocatalytic no oxidation and in situ drifts studies," *The Journal of Physical Chemistry C*, vol. 121, pp. 12168–12177, 2017.

[15] H. Huang, K. Xiao, F. Dong, J. Wang, X. Du, and Y. Zhang, "Sulfur-doping synchronously ameliorating band energy structure and charge separation achieving decent visible-light photocatalysis of Bi2O2CO3," *RSC Advances*, vol. 6, no. 97, pp. 94361–94364, 2016.

[16] J. Xu, K. K. Wang, T. Liu, Y. Peng, and B. G. Xu, "Br-Doped $Bi_2O_2CO_3$ exposed (001) crystal facets with enhanced photocatalytic activity," *Crystengcomm*, vol. 19, no. 34, pp. 5001–5007, 2017.

[17] N. Liang, M. Wang, L. Jin et al., "Highly Efficient Ag_2O/$Bi_2O_2CO_3$ p-n Heterojunction Photocatalysts with Improved Visible-Light Responsive Activity," *ACS Applied Materials & Interfaces*, vol. 6, pp. 11698–11705, 2014.

[18] S. Peng, L. Li, H. Tan et al., "Monodispersed Ag nanoparticles loaded on the PVP-assisted synthetic Bi 2O2CO3 microspheres with enhanced photocatalytic and supercapacitive performances," *Journal of Materials Chemistry A*, vol. 1, no. 26, pp. 7630–7638, 2013.

[19] R. Wang, X. Li, W. Cui, Y. Zhang, and F. Dong, "In situ growth of Au nanoparticles on 3D Bi2O2CO3 for surface plasmon enhanced visible light photocatalysis," *New Journal of Chemistry*, vol. 39, no. 11, pp. 8446–8453, 2015.

[20] X. Meng and Z. Zhang, "Pd-doped Bi2MoO6 plasmonic photocatalysts with enhanced visible light photocatalytic performance," *Applied Surface Science*, vol. 392, pp. 169–180, 2017.

[21] X. Meng and Z. Zhang, "Bi2MoO6 co-modified by reduced graphene oxide and palladium (Pd2+ and Pd0) with enhanced photocatalytic decomposition of phenol," *Applied Catalysis B: Environmental*, vol. 209, pp. 383–393, 2017.

[22] X. Meng, Z. Li, J. Chen, H. Xie, and Z. Zhang, "Enhanced visible light-induced photocatalytic activity of surface-modified BiOBr with Pd nanoparticles," *Applied Surface Science*, vol. 433, pp. 76–87, 2018.

[23] X. Meng, Z. Li, and Z. Zhang, "Pd-nanoparticle-decorated peanut-shaped $BiVO_4$ with improved visible light-driven photocatalytic activity comparable to that of TiO2 under UV light," *Journal of Catalysis*, vol. 356, pp. 53–64, 2017.

[24] P. Yang, C. Lu, N. Hua, and Y. Du, "Titanium dioxide nanoparticles co-doped with Fe^{3+} and Eu^{3+} ions for photocatalysis," *Materials Letters*, vol. 57, no. 4, pp. 794–801, 2002.

[25] X. Meng and Z. Zhang, "Plasmonic Z-scheme Ag2O-Bi2MoO6 p-n heterojunction photocatalysts with greatly enhanced visible-light responsive activities," *Materials Letters*, vol. 189, pp. 267–270, 2017.

[26] W. Kohn and L. J. Sham, "Self-consistent equations including exchange and correlation effects," *Physical Review A: Atomic, Molecular and Optical Physics*, vol. 140, no. 4A, pp. A1133–A1138, 1965.

[27] J. P. Perdew, J. A. Chevary, S. H. Vosko et al., "Atoms, molecules, solids, and surfaces: Applications of the generalized gradient approximation for exchange and correlation," *Physical Review B: Condensed Matter and Materials Physics*, vol. 46, no. 11, pp. 6671–6687, 1992.

[28] P. Giannozzi, S. Baroni, N. Bonini et al., "QUANTUM ESPRESSO: a modular and open-source software project for quantum simulations of materials," *Journal of Physics: Condensed Matter*, vol. 21, no. 39, Article ID 395502, 2009.

[29] C. Greaves and S. K. Blower, "Structural relationships between Bi2O2CO3 and β-Bi2O3," *Materials Research Bulletin*, vol. 23, no. 7, pp. 1001–1008, 1988.

[30] X. Shang, W. Lu, B. Yue et al., "Synthesis of three-dimensional hierarchical dendrites of NdOHCO3 via a facile hydrothermal method," *Crystal Growth and Design*, vol. 9, no. 3, pp. 1415–1420, 2009.

[31] Y. Yu, T. He, L. Guo et al., "Efficient visible-light photocatalytic degradation system assisted by conventional Pd catalysis," *Scientific Reports*, vol. 5, article no. 9561, 2015.

[32] H. Lu, L. Xu, B. Wei, M. Zhang, H. Gao, and W. Sun, "Enhanced photosensitization process induced by the p-n junction of Bi 2O2CO3/BiOCl heterojunctions on the degradation of rhodamine B," *Applied Surface Science*, vol. 303, pp. 360–366, 2014.

[33] T. Wu, G. Liu, J. Zhao, H. Hidaka, and N. Serpone, "Photoassisted Degradation of Dye Pollutants. V. Self-Photosensitized Oxidative Transformation of Rhodamine B under Visible Light

Irradiation in Aqueous TiO_2 Dispersions," *The Journal of Physical Chemistry B*, vol. 102, pp. 5845–5851, 1998.

[34] T. Li, L. Zhao, Y. He, J. Cai, M. Luo, and J. Lin, "Synthesis of g-C_3N_4/$SmVO_4$ composite photocatalyst with improved visible light photocatalytic activities in RhB degradation," *Applied Catalysis B: Environmental*, vol. 129, no. 17, pp. 255–263, 2013.

[35] G. Li, B. Jiang, S. Xiao et al., "An efficient dye-sensitized BiOCl photocatalyst for air and water purification under visible light irradiation," *Environmental Science: Processes & Impacts*, vol. 16, pp. 1975–1980, 2014.

[36] S. Linic, P. Christopher, and D. B. Ingram, "Plasmonic-metal nanostructures for efficient conversion of solar to chemical energy," *Nature Materials*, vol. 10, no. 12, pp. 911–921, 2011.

[37] W. Hou and S. B. Cronin, "A review of surface plasmon resonance-enhanced photocatalysis," *Advanced Functional Materials*, vol. 23, no. 13, pp. 1612–1619, 2013.

[38] R. Asahi, T. Morikawa, T. Ohwaki, K. Aoki, and Y. Taga, "Visible-light photocatalysis in nitrogen-doped titanium oxides," *Science*, vol. 293, no. 5528, pp. 269–271, 2001.

[39] A. Sobczyński, L. Duczmal, and W. Zmudziński, "Phenol destruction by photocatalysis on TiO2: An attempt to solve the reaction mechanism," *Journal of Molecular Catalysis A: Chemical*, vol. 213, no. 2, pp. 225–230, 2004.

[40] K. Momma and F. Izumi, "VESTA 3 for three-dimensional visualization of crystal, volumetric and morphology data," *Journal of Applied Crystallography*, vol. 44, no. 6, pp. 1272–1276, 2011.